# Measurement of Photovoltaic Module Deformation Dynamics During Hail Impact Using Digital Image Correlation

James Y. Hartley, Michael A. Shimizu, Jennifer L. Braid, Ryan Flanagan, Phillip Reu

Sandia National Laboratories, Albuquerque, New Mexico, 87185, United States

Abstract-Stereo high-speed video of photovoltaic modules undergoing laboratory hail tests was processed using digital image correlation to determine module surface deformation during and immediately following impact. The purpose of this work was to demonstrate a methodology for characterizing module impact response differences as a function of construction and incident hail parameters. Video capture and digital image analysis were able to capture out-of-plane module deformation to a resolution of  $\pm 0.024$ mm at 11 kHz, on an in-plane grid of 10 mm x 10 mm over the area of a 1 x 2 m commercial photovoltaic module. With lighting and optical adjustments, the technique was adaptable to arbitrary module designs, including size, backsheet color, and cell interconnection. Impacts were observed to produce an initially localized dimple in the glass surface, with peak deflection proportional to the square root of incident energy. Subsequent deformation propagation and dissipation were also captured, along with behavior for instances when the module glass fractured. Natural frequencies of the module were identifiable by analyzing module oscillations post-impact. Limitations on the measurement technique were that the impacting ice ball obscured the data field immediately surrounding the point of contact, and both ice and glass fracture events occurred within 100µs which was not resolvable at the chosen frame rate. Increasing frame rate and visualizing the back surface of the impact could be applied to avoid these issues. Applications for these data include validating computational models for hail impacts, identifying the natural frequencies of a module, and identifying damage initiation mechanisms.

Keywords—hail impact, digital image correlation, finite element modeling, mechanical testing

#### I. INTRODUCTION

Large hail weather events pose an increasingly significant risk to photovoltaic installations, as deployments continue to colonize additional land area and service life targets up to 50 years [1] approach or exceed local frequencies for large hail events [2]. Module design and qualification must therefore consider hail impact events as an expected lifetime exposure, and accordingly various test protocols have been implemented addressing module resiliency using laboratory ice balls [3],[4].

Funding provided as part of the Durable Modules Consortium (DuraMAT), an Energy Materials Network Consortium funded by the U.S. Department of Energy, Office of Energy Efficiency and Renewable Energy, Solar Energy Technologies Office. The views expressed in the article do not necessarily represent the views of the DOE or the U.S. Government. The U.S. Government retains and the publisher, by accepting the article for publication, acknowledges that the U.S. Government retains a nonexclusive, paid-up, irrevocable, worldwide license to publish or reproduce the published form of this work, or allow others to do so, for U.S. Government purposes.

However, existing test protocols typically only produce a pass or fail result based on visible damage (i.e., glass cracking) and therefore do not account for susceptibility to cell cracking. Furthermore, these standards bin modules by survival of ice ball diameter classes from 25 to 85 mm, which causes most modules to be categorized at the same resiliency level even when nuances in survivability may exist. Methods or techniques for fully characterizing module hail resiliency beyond the resolution provided by standardized testing could help to refine module selection and insurance practices for hail-prone installations.

Computational simulations of hail impacts are one approach for quantifying the potential for damage, by allowing the full dynamics and stress states during impact to be analyzed and compared across module designs [5]. However, validation of predicted quantities against an experimentally measurable metric is required for full confidence in model accuracy. Contrarily, probabilistic experiments conducted over a sufficiently large sample set can produce a definitive probability of module failure for a tested ice ball class [6] but cannot provide mechanistic explanations for the observation. An experimental measurement technique for characterizing module behavior during impact is therefore of interest, to validate and enable full utilization of simulation insights and provide additional physical observations to support damage probability results.

Digital image correlation (DIC) is a well-established, commercially available technique [7],[8] for measuring displacements on a subject of interest based on the movements of image features, a known reference calibration, and optical geometries. Measurement success is limited by the combination of visual accessibility of the test subject and event characteristics relative to camera capabilities, such as frame rate, resolution, and environmental survivability. Since laboratory hail tests against PV modules are not stressing to these factors, DIC was expected to be a suitable technique for capturing and characterizing the impact event.

In this study, DIC is applied to stereo high-speed video of laboratory hail tests against PV modules, to produce measurements of module front surface deformation in the moments during and after impact. The primary goal of this work was to acquire spatially and temporally resolved data for computational model validation. Additional applications for time-dependent displacement data could be to analyze and explain impact damage trends to inform future module design improvements, and to characterize module frequency response

to better understand dynamic failure modes related to module and tracker wind loading [9].

## II. METHODS

# A. Hail testing setup

The hail testing apparatus was based on an IEC-compliant [3] setup (Fig. 1) consisting of a pressure-modulated pneumatic cannon with interchangeable barrels for ice ball diameters of 25 to 85 mm in increments of 10 mm. Velocity measurement was obtained via two timed optical gates at the muzzle spaced 100 mm apart. Ice ball casting, temperature hold, and loading procedures were also based on IEC definitions [3], although to accommodate the camera and lighting setup for DIC, total distance from cannon muzzle to module surface was increased to approximately 2.5 meters. Module mounting utilized actual PV structural railing and clamps [10] at module interfaces, with the remainder of the structure built from modular aluminum extrusions.

## B. Videography setup and data acquisition procedure

# 1) Module patterning for image correlation

Two methods for module surface patterning were explored, to provide reference features for DIC. The first was solvent-based flat white enamel spray paint, applied through a plastic stencil, while the second was water-based flat white acrylic liquid paint, applied with a foam roller over the same stencil. The distinction between paints was to facilitate removability for subsequent electroluminescence and solar simulator testing, which require a clean glass surface, for which the acrylic paint was preferred, though no differences were observed in DIC performance between paints. The stencil speckle size was 6.35 mm with a density of ~50% coverage, yielding image feature diameters of approximately 5 pixels.

## 2) Cameras, lighting, and test procedures

A stereo imaging setup was used consisting of two Phantom v2640 cameras operated at 11,000 frames per second and 1920x1200 pixel resolution, each equipped with 18-35 mm lenses. Cameras were positioned approximately 1 m forward of the hail cannon, with plastic bags providing protection from water and ice spray. Aluminum structural railing was used to fix cameras at their relative positions as a rigid assembly on a crossbeam supported by heavy-duty tripods. The final imaging setup is shown in Fig. 1, placing the cameras at the module midheight, approximately 1.5 meters away from the glass and forming an angle of roughly 25 degrees to each other. For this configuration, lenses were set to approximately 20 mm focal length and f-number 5.6 to optimize the depth of field to sharpness ratio. Camera frame synchronization was verified with an oscilloscope to less than 1 µs which was adequate for the expected surface velocities encountered in the tests.

Lighting was achieved with four 200 W LED panels, each with an output of approximately 25,000 lumens, along with white polystyrene insulation boards and plastic sheeting for reflecting and diffusing. Significant tuning was needed to achieve suitable lighting, based on a strategy of combining high-angle direct lighting with diffuse lighting to reduce specular reflection and glare. Module visual appearance (e.g.

white vs. black vs. clear backsheet, cell gap dimensions, interconnection type) affected the lighting solution but were accommodatable with adjustment.





Fig. 1. Hail testing setup with high speed video acqusition equipment.

For each tested module, a camera calibration was first performed using a Correlated Solutions 36" x 24" 56mm calibration target board and VIC-3D 9 software. Thereafter, static images of the module were acquired to verify the regions of interest were adequately registered. Hail shots were then executed with video acquisition during impact and in-situ postimpact EL imaging to assess module damage.

## C. Digital image analysis

Acquired videos were converted to sequential Tag Image File (.tif) images and analyzed using VIC-3D 9 software for DIC. Stereo images were matched, low-pass filtered, and coevaluated with subset size of 41 and step size of 10 pixels using Gaussian weighting and an affine shape-function.

Accuracy limits for in- and out-of-plane deflection are determined by the software based on the subset and step sizes and quality of matching. For a 1-standard-deviation confidence interval on position, the combination of pixel confidence margin and camera setup for the test series resulted in an average subset matching confidence interval less than 0.007

pixels, translating to an in-plane deflection average uncertainty of  $\pm 0.009$  mm and out-of-plane average uncertainty of  $\pm 0.024$  mm. This resolution is more than adequate to capture out-of-plane deformations over correlated regions of the module glass (Fig. 2). To facilitate direct analysis of deformed module shapes, surface deformations were used instead of absolute positions, to ignore initial distortions in the unstressed module and assume an initially flat state. Data was further resized to a 10 mm x 10 mm grid to reduce computational time in surface fitting and analysis, since additional resolution produced irrelevant data on surface texture and noise.

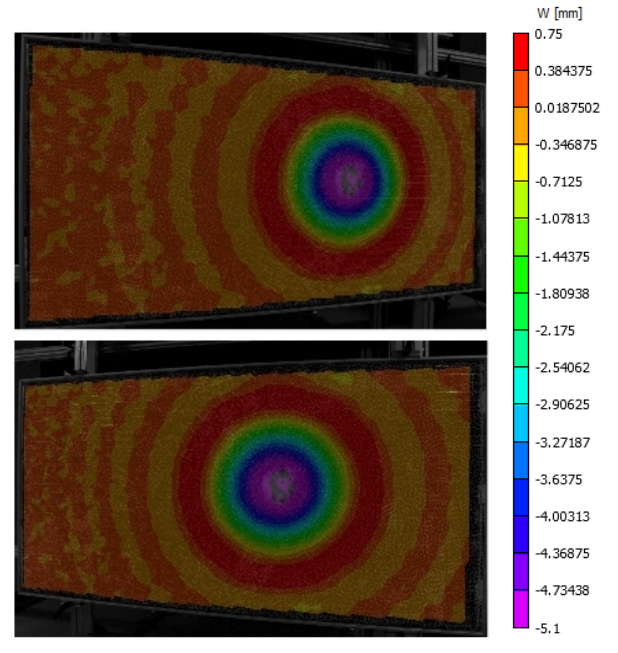


Fig. 2. Left and right camera views of a 1 x 2 m format test module overlaid with correlated area and colored by out-of-plane displacement. As shown: 1.9 ms after a 65 mm ice ball impact at 34.48 m/s.

## III. RESULTS

# A. Ice ball impact identification and data interpolation

Fig. 3 shows a frame-by-frame progression of a 55 mm ice ball impacting against a 72-cell glass backsheet module from raw video prior to DIC. The ice ball can be seen to transition from clear to opaque upon contact and fracture, allowing the moment of contact to be identified temporally to within 1 frame  $(1/11,000\ \text{second})$ , and spatially on the plane of the module to approximately  $\pm 2\ \text{mm}$  limited by ice ball sphericity.

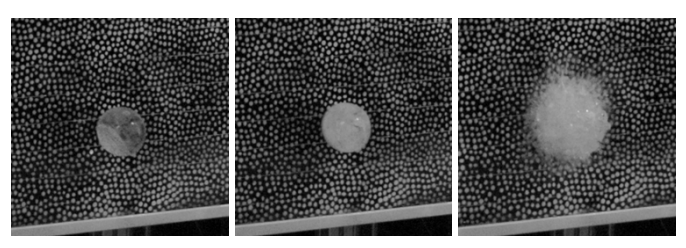


Fig. 3. Frame-by-frame progression of ice ball contacting module. Impact time and location were identifiable to within 1/11,000 second and approximately ±2 mm, respectively.

Since ice ball fragmentation obscured the module patterning underneath the impact site, no DIC data was available in the immediate vicinity of the ice ball as shown Fig. 4. To estimate the missing data field in each frame, a fourth order 2D polynomial interpolation was constructed using the surrounding 50 x 50 array of points, first as a fit to all points and then refitted excluding outliers with a relative error >10% from the initial fit. R-squared values for this method were greater than 0.98, suggesting that a good representation of the waveform around the impact was achieved.

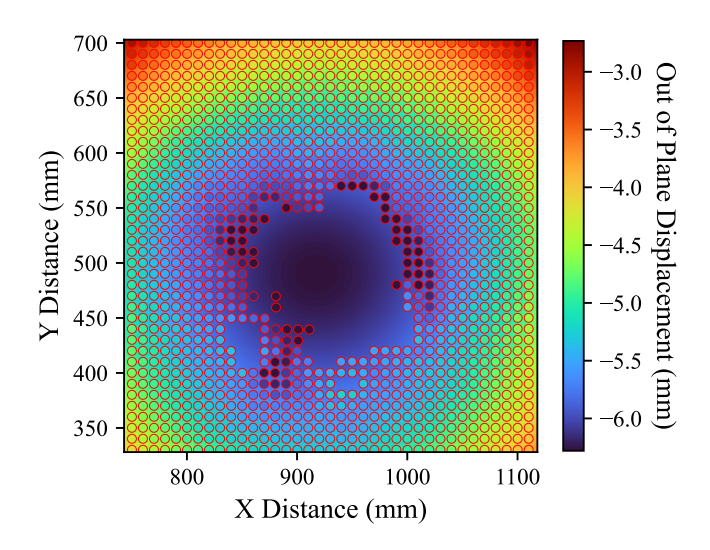


Fig. 4. Measured and interpolated out-of-plane displacement data in the immediate vicitinity of an ice ball impact. Markers are colored by measured displacement value, with missing markers indicating obscured DIC data. Background is colored by interpolation solution. Marker color matching background color indicates a strong correlation. As shown: 65 mm ice @ 35.21 m/s, 48.71 J.

# B. Module impact analysis, center impact

Fig. 5 shows a typical deformation progression during a 55 mm ice ball impact to the center of the module, when glass remains intact. A localized circular dimple with 4 mm peak deflection into the module plane is visible 1 ms after initial contact. The affected area spreads outward at approximately 100 m/s, determined by tracking the circular band of ~1 mm out-of-plane displacement in Fig. 5. By 7 ms after contact, the rate of propagation has decayed, and the affected radius becomes less distinct as the full module area has been affected. Thereafter, reflections and oscillations continue to occur at varying magnitudes throughout the module plane. The largest displacement gradients occur immediately post impact, suggesting that glass strain is largest early in the impact event, though strains later in the event are still a similar magnitude as strains measurable during uniform static loading [11]. This implies that the largest mechanical stress and damage likelihood occurs immediately following impact underneath the impact location, but subsequent dynamics can still produce local strains comparable to a static loading exposure and be of interest for cell crack initiation or propagation.

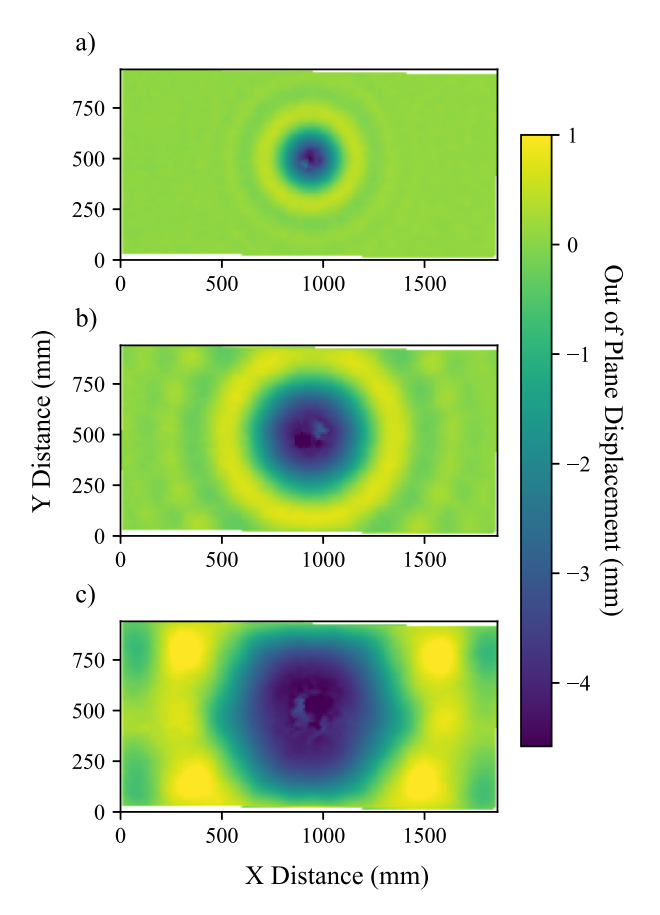


Fig. 5. Sequential visualization of module deformations during an ice ball impact against the center of the module, at a) 1 ms b) 3 ms and c) 7 ms after initial contact, with glass remaining intact throughout impact. 55 mm ice ball @ 33.33 m/s, 44.14 J shown.

# C. Module impact analysis, edge adjacent

Fig. 6 shows a 55 mm ice ball impact near the module frame, when glass remains intact. The same initial deformed profile is observed at 1 ms with similar absolute magnitudes as the center impact, suggesting that early deformation response is dictated by the laminate materials alone since the impact disturbance has not yet reached the frame. Subsequent propagation is limited by the module edge and forms a truncated profile compared to the center impact seen in Fig. 5, placing larger strains on the glass edge at the constraint.

# D. Module deformation vs. ice ball energy

Additional impacts against the center of the module were characterized using DIC and interpolated to find maximum displacement into the module plane as a function of incident ice ball energy. Results are shown in Fig. 7, for incident energies representative of 40 – 65 mm ice balls per IEC hail test standards [3]. For the 3.2 mm glass-backsheet module of interest, an approximately square root relation was found, from 0 origin to 6.3 mm of peak displacement at 73 J incident energy. In addition to the deformation surface profiles shown in Fig. 5 and Fig. 6., this can help to provide computational model validation data across a range of relevant ice ball sizes.

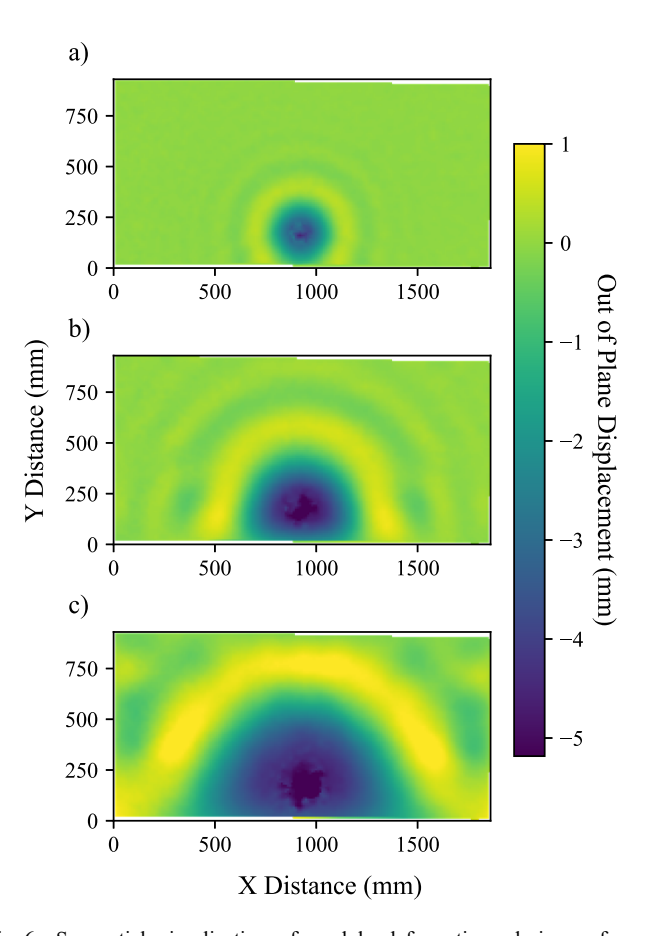


Fig. 6. Sequential visualization of module deformations during a frame-adjacent ice ball impact, at a) 1 ms b) 3 ms and c) 7 ms after initial contact, with glass remaining intact throughout impact. 55 mm ice ball @ 33.11 m/s, 42.59 J shown.

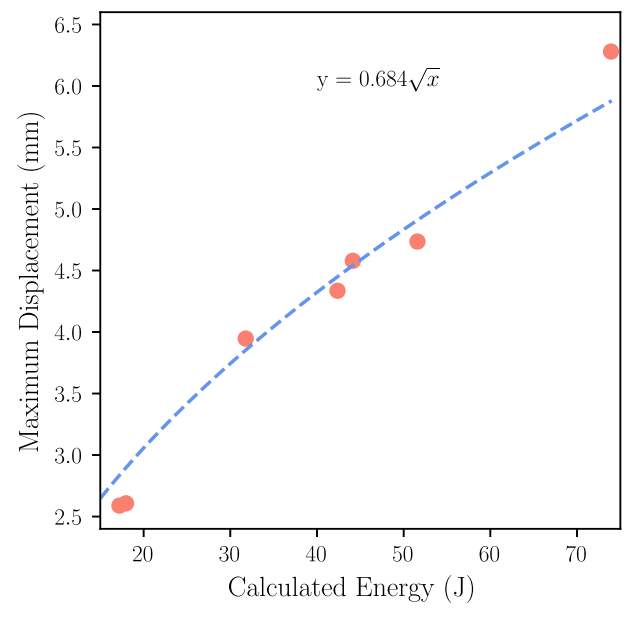


Fig. 7. Interpolated module peak deformation vs. hail incident energy from DIC testing, forming an approximately square root relation.

# E. Module impacts with glass failure

For impacts resulting in glass failure, cracks were evident within 2 video frames (2/11,000 second) after contact, consistent with deformation observations suggesting that peak stresses occur in the immediate vicinity of initial contact. Cracks first appeared as a concentric ring of disturbed glass around the ice ball, identifiable by subtracting the initial contact image at time 0 s from subsequent frames (Fig. 8). Due to the indistinct appearance of broken tempered glass, it is possible that the initial failure occurred even sooner or was obscured by the ice ball. However, a key observation was that glass failure occurs prior to any significant surface deformation (Fig. 5 and Fig. 6) and is therefore a locally initiated phenomenon.

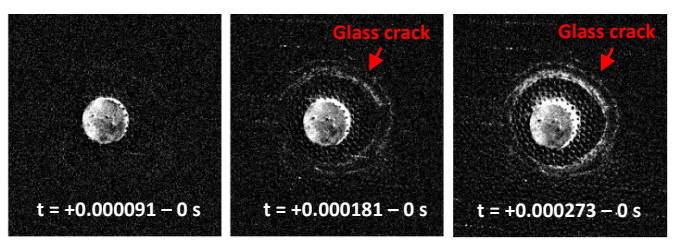


Fig. 8. Sequential image differentials of an ice impact with glass failure, initial contact at t=0 s. Left: ice ball transitioned to opaque but no apparent glass failure. Center and right: Visible glass failure pattern denoted with arrow.

Surface deformation profiles from modules exhibiting glass failure are shown in Fig. 9. The same patterns are seen for both center and edge adjacent impacts, though deformation magnitudes of 15-30 mm into the initial glass plane indicate permanent damage.

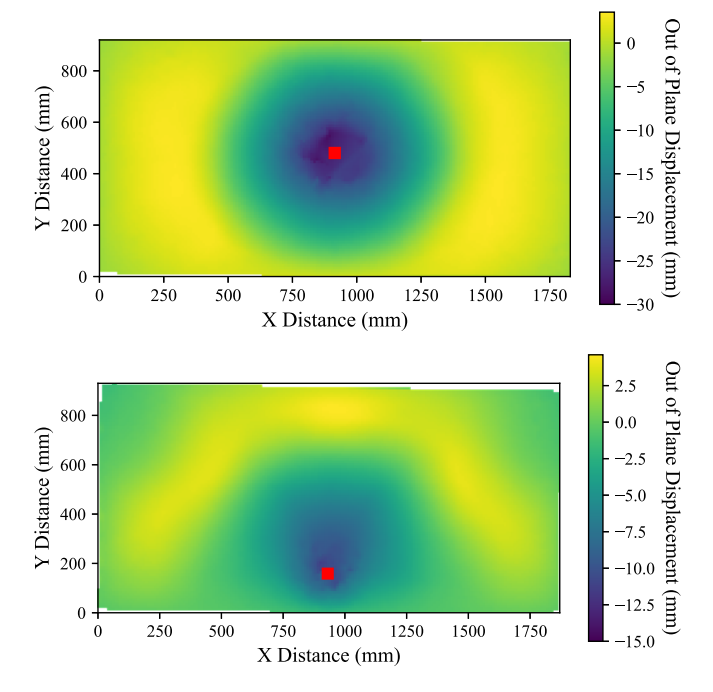


Fig. 9. Module deformations for impacts resulting in glass failure. Top: 75 mm ice ball @38.46 m/s, 141.78 J; bottom: 55mm ice ball @ 34.01m/s, 42.97 J.

# F. Module dynamic response

To analyze post-impact module dynamics and frequency response, a series of longer, ~750 ms post-impact videos were

collected for impacts against a 60-cell, 3.2 mm glass-backsheet module. A 35 mm ice ball size was used to provide an initial excitation without risk of breaking the module glass. Mounting configuration was like Fig. 1 at four distributed clamping points, though with the long edge oriented vertically. Fig. 10 shows averaged and low-pass filtered out-of-plane deflection on the front glass surface computed with DIC, showing oscillation into and out of the initial surface plane at a discernable frequency, decaying to 0 over an apparent time of approximately 2 seconds.

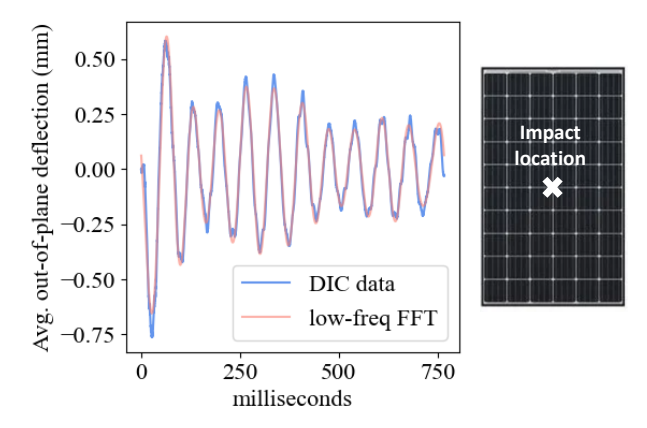


Fig. 10. Average out-of-plane glass displacement after a center ice ball impact, overplotted with a low-pass filter. 35 mm ice ball @31.15 m/s, 9.84 J.

Fig. 11 shows a low-pass Fourier transform of the time domain deformation response shown in Fig. 10, along with 5 additional 35 mm ice ball impacts directed at the module center and top and bottom halves. Dominant frequency can be seen to be 14.4 Hz with a secondary peak at 11.5 Hz. Since these frequencies occurred independently of ice impact location, they can be attributed to the natural frequency  $\omega_0$  of the module based on its overall mass and stiffness, per the classical mechanics relation [12] for a spring-mass system of stiffness k and mass m (Eqn. 1).

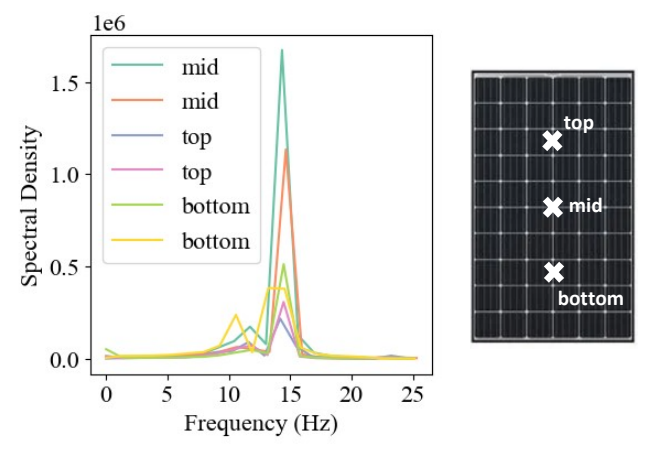


Fig. 11. Spectral density of average surface displacement vs. time for various 35 mm ice ball impacts. A primary characteristic frequency at 14.4 Hz is apparent, with a secondary peak at 11.5 Hz.

Notably, the ratio of characteristic frequencies was nearly identical to the square of the module edge dimensions of 1 m x 1.6 m, suggesting that the 14.4 Hz component was due to oscillations along the module short dimension and the 11.5 Hz

component was due to the module long dimension per Eqn. 1 with mass held constant but assuming the module has independent stiffness contributions from each edge.

$$\omega_0 = \sqrt{k/m} \tag{1}$$

These findings suggest that larger format modules such as 1 m x 2 m of similar laminate and frame construction could expect an analogous natural frequency near 14.4 Hz for their 1 m short dimension, potentially reduced due to larger mass, but also a lower secondary frequency of ~10.2 Hz due to the larger side length ratio. If parameters such as frame stiffness or glass thickness are reduced, even lower frequencies could be expected. Although not significantly relevant for hail impact damage assessment, the ability to identify module natural frequencies is another potential application for DIC. The presence of natural frequencies on the order of 10 Hz or less may be of interest for assessing module robustness against oscillatory wind loads, which are known to occur in a similar frequency range [9],[13].

# IV. SUMMARY AND CONCLUSIONS

In this work we demonstrate the use of DIC to analyze module deformation dynamics during simulated hail impact tests. Setup and equipment parameters for successful data acquisition were presented along with test and analysis procedures. Key findings were:

- Measurement accuracy was ±0.009 mm and ±0.024 mm in- and out-of-plane, respectively, over the full 1 m x 2 m module surface. This was near the upper limit for 1920x1200 pixel cameras, with slight potential improvements possible by altering setup geometries.
- Impact timing within a video sequence was clearly identifiable by the ice ball transitioning from clear to opaque upon fracture. However, this transition was fully complete within 1 frame at the selected rate of 11,000 Hz, which limits how precisely initial ice ball contact time can be found. Additional resolution up to ~100,000 Hz would be beneficial to observe and characterize ice ball fracture.
- The visual obstruction produced by the ice ball at the impact site was a limiting factor for data completeness. This was noteworthy since glass fracture was observed to occur within 1-2 frames, initiating near the point of contact, but further localization (both temporal and spatial) was not possible since the selected frame rate was low and the image was obscured. Future studies on the module back surface at a higher frame rate could be beneficial to better characterize fracture behavior. For impacts without glass fracture, a polynomial interpolation provided a strongly correlated match to available points surrounding the obscured field, indicating a credible representation of the missing data.

Module frequency response as excited by hail impacts was measurable using DIC, with distinct natural frequencies identified at 11.5 and 14.4 Hz for a 60-cell glass backsheet module. Adequate measurements could be made using conventional camera frame rates and may be of interest for assessing module robustness against vibrations induced by oscillatory wind loading.

#### V. ACKNOWLEDGMENT

The authors thank Doug Robb and Colin Sillerud at CFV Labs for their assistance in test design and execution.

Sandia National Laboratories is a multimission laboratory managed and operated by National Technology and Engineering Solutions of Sandia, LLC, a wholly owned subsidiary of Honeywell International Inc., for the U.S. Department of Energy's National Nuclear Security Administration under contract DE-NA0003525.

This paper describes objective technical results and analysis. Any subjective views or opinions that might be expressed in the paper do not necessarily represent the views of the U.S. Department of Energy or the United States Government.

#### VI. REFERENCES

- FY22 Annual Report. Durable Module Materials Consortium. NREL/BR-5K00-85350. Feb. 2023. <a href="https://www.nrel.gov/docs/fy23osti/85350.pdf">https://www.nrel.gov/docs/fy23osti/85350.pdf</a>
- [2] Severe Weather Maps, Graphics, and Data Page. National Oceanic and Atmospheric Admnistration Storm Prediction Center. Apr. 2023. https://www.spc.noaa.gov/wcm/
- [3] Terrestrial photovoltaic (PV) modules Design qualification and type approval. MQT 17: Hail Test. IEC 61215-1-1:2016. 2016.
- [4] Standard test Method for Determining Resistance of Photovoltaic Modules to Hail by Impact with Propelled Ice Balls. ASTM E1038-10. 2019.
- [5] J. Hartley, J. Braid, C. Sillerud. "Analyzing hail impacts on PV modules using computational simulation". 2023 Photovoltaics Reliability Workshop. Lakewood, CO, USA. Mar. 2023.
- [6] G. Spina, K. Bhatti, C. Moffet, J. Rolak, L. Trippel. "Hail Impact Energy Resilience Threshold Testing". Photovoltaics Reliability Workshop. Lakewood, CO. 2023.
- [7] P. L. Reu, T. J. Miller. "The application of high-speed digital image correlation". *The Journal of Strain Analysis for Engineering Design*. 2008;43(8):673-688. doi:10.1243/03093247JSA414J.
- [8] E.M. Jones and M. A. Iadicola (Eds.). "A Good Practices Guide for Digital Image Correlation". International Digital Image Correlation Society, 2018. DOI: 10.32720/idics/gpg.ed1
- [9] D. Kresse. "High Wind Speed PV Module Failures". 2022 NREL Photovoltaics Reliability Workshop. Feb. 2022.
- [10] Module Clamps for Framed Modules. Schletter North America 2023/3 Product Catalog. Nov. 2023. https://www.schletter-group.com/mountingsystems/product-catalog/
- [11] A. Maes, et al., "Instrumented Modules for Mechanical Environment Characterization and Simulation Model Validation," 2020 47th IEEE Photovoltaic Specialists Conference (PVSC), 2020, pp. 1525-1530, doi: 10.1109/PVSC45281.2020.9300468.
- [12] J. L. Meriam and L.G, Kraige. Engineering Mechanics: Dynamics 6<sup>th</sup> Edition. Hoboken, New Jersey: John Wiley & Sons. 2007. pp. 603.
- [13] Aßmus, M. & Jack, Steffen & Weiss, Karl-Anders & Köhl, Michael. (2011). Measurement and simulation of vibrations of PV-modules induced by dynamic mechanical loads. Progress in Photovoltaics: Research and Applications. 19. 688-694. 10.1002/pip.1087. simulations". Prog. Photovolt: Res. Appl., 25: 791–809. 2017. doi: 10.1002/pip.2891.